Theor Chem Acc (2006) 116: 124–136
DOI 10.1007/s00214-005-0016-x

REGULAR ARTICLE

Kevin M. Rosso · Michel Dupuis

Electron transfer in environmental systems: a frontier for theoretical chemistry

Received: 31 March 2005 / Accepted: 30 August 2005 / Published online: 19 October 2005

Abstract The advances in understanding the kinetic behavior of certain environmental electron transfer (ET) systems are presented. Emphasis is placed on the homogeneous ET chemistry of transition metals, particularly the $Fe^{II/III}$ system, in various relevant forms. In the context of modern ET theory, we examine the utility of computational chemistry methods for the calculation of ET quantities such as the reorganization energy and electronic coupling matrix element. We discuss successful application of the methods to topics of homogeneous oxidation of dissolved metal ions by molecular oxygen in aqueous solution, as well as the prediction of electron mobility in solid phase iron oxide crystals. The examples illustrate the significant potential for many more advances in understanding environmental ET systems through the combination of ET theory and computational chemistry.

Keywords Electron transfer · Iron · Manganese · Polaron · Electronic coupling matrix element · Reorganization energy

1 Introduction

The description of the chemistry of natural waters almost always involves, by necessity, the influence of electron transfer (ET) reactions on the system. This includes an extremely diverse range of possible mechanistic pathways, including abiotic and biotic, homogeneous and heterogeneous, spontaneous and photochemical ET. Moreover, we often find ET reactions to be important in natural water systems, because of their slowness. The processes in natural waters that hinge directly upon the facility with which electrons can be transferred (i.e. the ET rate) include the movement of redox-sensitive metals such as Fe and Mn [1], the respiration of dissimilatory metal-reducing bacteria [2] and the related role of electron shuttle molecules [3–5], and the reductive dissolution of metal oxide minerals [6,7]. In addition to the vast array of natural ET processes, we have many important man-made environmental challenges in which ET rates are in direct control of the fate of anthropogenic contaminants. Examples in this category include the immobilization and recovery of redox-active toxic metals and radionuclides [8–11], and the reductive/oxidative degradation of organic solvents and pesticides [12–16]. Owing to the lack of a better descriptor, we refer to the collective cornucopia of possible natural and contaminant ET systems in natural waters as 'environmental ET systems'.

Given the importance of environmental ET systems, it is surprising that very little quantitative information is known about them at a fundamental level, even for the most central ones. The scientific lineage of modern ET theory stems from a few identifiable starting points, with great forward advances occurring way back from 1950s [17–20]. Thus, for more than 50 years, there have been only a few instances in which basic ET theory has been applied specifically to environmental ET systems. Therefore, it is possible to identify certain systems where the application of ET theory would immediately be very fruitful for improving our scientific understanding. This is especially true in light of the current widespread use of computational chemistry methods for simulation of elementary chemical reactions in general.

One such environmental ET system is the slow oxidation of Mn^{II} by oxygen in aqueous solution, a principal process regulating the rate of manganese cycling in natural waters. Thermodynamically, the most stable form of Mn in the presence of oxygen is in a solid phase oxide [21]. However, the homogeneous abiotic oxidation ET reaction has been shown to be kinetically inhibited for time periods on the scale of months [22]. There are many reports of experimental measurements of the homogeneous oxidation kinetics of aqueous metal ions such as Fe^{II} [23–30], Mn^{II} [22,31–33], and Cr^{II} [34–36]. The list grows significantly if the catalytic roles of solid mineral surfaces or microbiologic activity is included. However, in all cases, the physical quantities controlling and differentiating the oxidation rates of the different metal ions remain poorly understood.

K. M. Rosso (✉) · M. Dupuis
Pacific Northwest National Laboratory P.O. Box 999,
K8-96 Richland, WA 99352, USA
E-mail: kevin.rosso@pnl.gov
Tel.: +1-509-3767762
Fax: +1-509-3763650

Another instance in which ET kinetics directly impact an environmental system is the hopping mobility of electrons in solid phase iron oxide minerals [37–41]. Hematite (α-Fe_2O_3) is one of the primary electron sinks for a wide range of environmental abiotic and biotic ET processes in natural waters. For example, the natural respiratory action of dissimilatory metal-reducing bacteria attached to hematite leads to reduction of Fe^{III} acceptor sites in the oxide phase [2]. The injection of electrons has the general outcome of converting Fe^{III} into Fe^{II} and, at an interface with solution, this is often coupled with dissolution of the hematite by release of Fe^{II}. One of the key mysteries is exactly how donated electrons are spatially and kinetically linked with release of Fe^{II} from the solid surface [42]. Pure hematite is anti-ferromagnetic below ~960 K [43,44] and has a charge transfer band gap of 2.2 eV [45,46]. The electrical properties of hematite have been the focus of many studies, starting with Morin [47]. Electrical conduction is attributed to the hopping of small polarons [48], whereby the ET occurs between spatially localized Fe(3*d*) electronic levels from one iron atom to another by $Fe^{II/III}$ valence alternation [49,50]. Despite the experimental coverage on this topic, only very few theoretical expositions of ET processes in solid phase iron oxides have been produced [40,51,52].

The purpose of the current paper can be stated simply. We wish to highlight advances that are being made specifically on environmental ET systems through the combined use of modern ET theory and ab initio computational chemistry calculations. For the sake of this, we review the physical quantities of ET theory and methods of their computation. This is followed by demonstration of successful application towards the two environmental ET systems mentioned above, namely, metal ion oxidation and charge mobility in hematite. Lastly, we conclude with a perspective on future directions.

2 Electron transfer model

The ET treatment discussed here is based on Marcus' two-state model [17], and many standard texts review the formalism presented below. We define the ET reactants as consisting of an electron donor (D) and an electron acceptor (A). For the moment, we need not define the environment in which the reactants exist, so the reactants could be, for example, a pair of solution species in an encounter complex, or neighboring metal sites in a solid phase, or a surface complex at a solid–liquid interface. Nor do we yet need to specify if the reactants are connected through shared bridging groups or not. However, close proximity of the reactants is implied. Hence, we denote the initial electronic state (also called the 'reactants state') as ψ_A=D···A and the final electronic state (also called the 'products state') as ψ_B=$D^+ \cdots A^-$, where '$\cdots$' indicates that the donor and acceptor are in close proximity on the scale of a few Ångstroms.

Electron transfer is a Franck-Condon process; electron motion is effectively instantaneous relative to the frequency of nuclear motion [53,54]. In order for the electron to move from donor to acceptor, the donor and acceptor energy levels must be brought into coincidence. The coincidence condition is achieved by reorganizing the nuclei of the reactant atoms and surrounding material to an appropriate configuration. Both the donor and acceptor are reconfigured, and this is accomplished spontaneously by thermal fluctuations. Because ET involves nuclear reorganization, we describe it in terms of potential energy surfaces as a function of collective nuclear coordinates, q. The initial and final states each may be assigned a diabatic potential energy surface, which are usually well approximated as parabolic with respect to q for small displacements in q (Fig. 1) [17]. The equilibrium initial and final state nuclear configurations (q_A and q_B) and energies are defined by the minima in the two potential energy surfaces. For ET with a free energy change upon going from the initial to the final states (ΔG°), the potential energy minima of the two states are vertically staggered (Fig. 1a). This case is sometimes referred to as an asymmetric ET reaction. A symmetric ET reaction has the condition ΔG°=0, wherein the potential energies at q_A and q_B are the same and the surfaces show a shape characteristic of a double well (Fig. 1b).

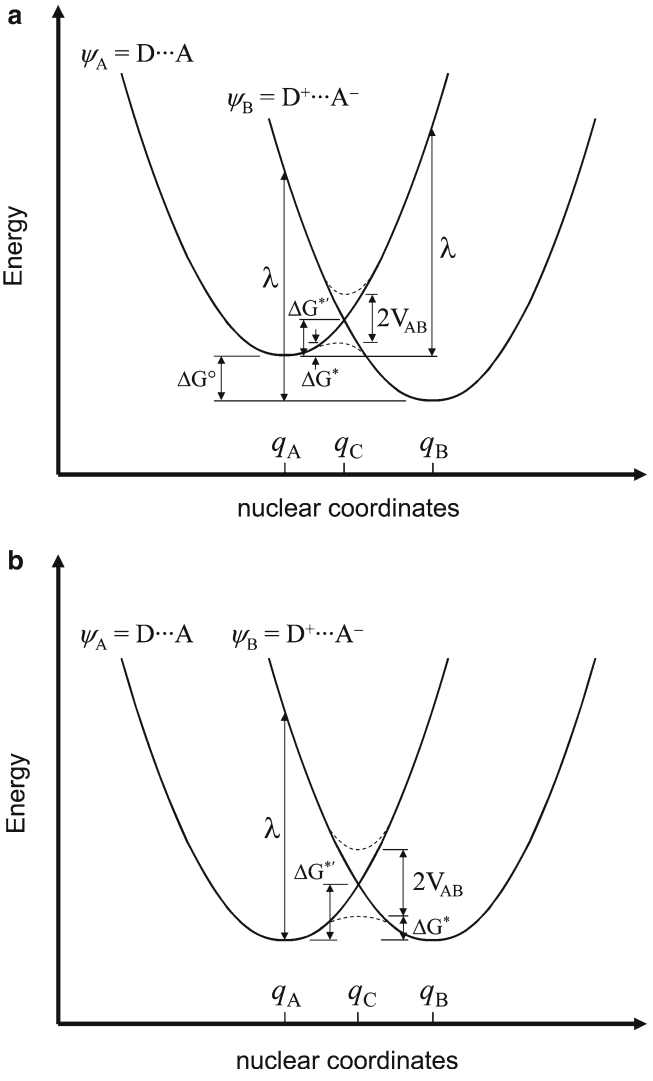

Fig. 1 Two-state potential energy diagrams showing the essential quantities of an **a** asymmetric and **b** symmetric ET process

In both the asymmetric and symmetric cases, thermally promoted ET proceeds by excitation to the crossing-point configuration q_C at the intersection between the two diabatic surfaces (Fig. 1). The energy at the intersection is the diabatic activation energy, labeled in Fig. 1 as $\Delta G^{*'}$. Note that the diabatic activation energy is different than activation energy ΔG^*, which will be discussed later.

Two important quantities now enter the ET model. The first is the reorganization energy λ, which is the energy to distort the equilibrium configuration of the reactants into the equilibrium configuration of the products, or vice versa, without having moved the electron (Fig. 1). In the case of symmetric ET, λ is equivalent to the energy to vertically excite the system from the initial electronic state to the final electronic state without changing the nuclear configuration. Thus, ET can occur by supplying the energy λ with light. For thermally promoted ET, $\Delta G^{*'} = \lambda/4$ for parabolic potential energy surfaces [17]. Therefore, λ is found in various possible expressions for the ET rate, as will be shown later. Marcus showed that λ often can be separated into two parts; the internal (or inner-sphere) part λ_I involving the energy to distort bonds in the reactants, and the external (or outer-sphere) part λ_E involving the energy to modify the polarization of the surrounding material due to the redistribution of charge in the internal part [17]. The total reorganization energy (hereafter λ) is then the sum of the two parts, $\lambda=\lambda_I+\lambda_E$. Also, not surprisingly, the separability of the two parts often turns out to be convenient in the design of a modeling strategy for their computation.

The second important quantity is the electronic coupling between the initial and final electronic states. At q_C, we are concerned with the electron tunneling probability between the initial and final states. This probability depends on the amount of electronic interaction between ψ_A and ψ_B at q_C. Such an interaction is quantified by the electronic coupling matrix element V_{AB}, which is given by

$$V_{AB} = \langle \psi_A | V(q_C) | \psi_B \rangle . \tag{1}$$

The quantity $V(q_C)$ is the effective perturbation operator that is responsible for the transition between states ψ_A and ψ_B at the intersection region. The electronic interaction causes a splitting to occur in the intersection region of magnitude $2V_{AB}$ (Fig. 1). If the interaction is weak and, therefore, V_{AB} is small (approximately $< kT$), the system will evolve on the reactants' surface for the most part upon excitation to q_C and at times tunnel onto the product surface. If the interaction is strong and, therefore, V_{AB} is large (approximately $> kT$), two new adiabatic states are formed from the diabatic ones (Fig. 1). In the adiabatic case, the system evolves on the lower surface and, barring multiple crossings over the barrier, impingement on q_C results in the ET products being formed. The weak interaction case is conventionally referred to as the 'nonadiabatic' (or also 'diabatic') case and the strong interaction case is referred to as 'adiabatic'.

Adiabaticity can be determined from the value of the transmission coefficient κ, which is given by [55,56]

$$\kappa = \frac{2P}{1+P}, \tag{2}$$

where P is the probability for conversion of the reactants into products upon a single passage through the intersection region. In the semiclassical model, P is given by [55]

$$P = 1 - \exp\left(-\frac{\nu_{el}}{2\nu_n}\right), \tag{3}$$

where ν_{el} is the frequency of ET at the intersection and ν_n is a nuclear vibration frequency. From the Landau–Zener model for classical harmonic motion [55,57,58]

$$\frac{\nu_{el}}{2\nu_n} = \frac{2\pi V_{AB}^2}{\hbar \nu \, |S_A - S_B|}, \tag{4}$$

where ν is the average velocity of the system moving through the intersection, and S_A and S_B are the slopes of the two potential energy surfaces at the intersection. For equivalent surfaces, as in the symmetric ET case, it can be shown that [55,59]

$$\nu_{el} = \frac{V_{AB}^2}{\hbar\pi}\sqrt{\frac{\pi^3}{\lambda kT}}. \tag{5}$$

For values of $\kappa << 1$, the ET reaction is nonadiabatic, whereas for κ=1 or nearly so, the ET reaction is considered adiabatic.

Given the knowledge of ΔG°, λ, and V_{AB}, it is possible to estimate the ET rate. Rate expressions differ depending on the adiabaticity, but generally have in common that the rate is proportional to the product of two probabilities, one being the probability of forming the nuclear configuration q_C, and the other being the electron transmission probability while at q_C. For the nonadiabatic case in the high-temperature limit, the ET rate can be taken as the golden rule-based expression [60]

$$k_{et} = \frac{2\pi}{\hbar} V_{AB}^2 \frac{1}{(4\pi\lambda kT)^{1/2}} \exp\left(\frac{-[\Delta G^\circ + \lambda]^2}{4\lambda kT}\right), \tag{6}$$

wherein it is assumed that the interaction between ψ_A and ψ_B is weak. For the adiabatic case, ignoring nuclear tunneling, the rate expression takes the form [17]

$$k_{et} = \kappa \nu_n \exp\left(\frac{-\Delta G^{*'}}{kT}\right). \tag{7}$$

In the case of similar parabolic potential energy surfaces, the diabatic activation energy is given by [17]

$$\Delta G^{*'} = \frac{(\Delta G^\circ + \lambda)^2}{4\lambda}. \tag{8}$$

Under similar assumptions, in the symmetric ET case, it is possible to estimate ΔG^* using [61]

$$\Delta G^{*'} = -\frac{\lambda}{4} + \frac{\left(\lambda^2 + 4V_{AB}^2\right)^{1/2}}{2} - V_{AB}. \tag{9}$$

In this case the adiabatic rate is given by

$$k_{et} = \nu_n \exp\left(-\frac{\Delta G^*}{kT}\right) \tag{10}$$

This treatment assumes that once the activation energy is overcome, the ET products will be formed.

Note in the above we have tacitly assumed that only classical nuclear modes contribute to the activation energy (i.e., $\hbar\nu_n \ll kT$), and that we can ignore the contribution of quantum modes (i.e., $\hbar\nu_n \gg kT$). For the specific applications covered below, we are primarily interested in the room-temperature behavior or higher, and we have found good performance in the classical assumption as shown below. Furthermore, in $Fe^{II/III}$ ET systems, we often are able to reduce the number of internal reorganizing modes that need to be considered to that of the breathing mode for Fe–O bonds.

3 Computational strategies

The main purpose of this section is to illustrate how computational chemistry methods can be used to estimate λ and V_{AB}. Such methods can also be used to estimate ΔG° for asymmetric ET reactions but we ignore this aspect here because calculation of free energy differences is not unique to ET reactions.

3.1 Internal reorganization energy

In general, there are two strategies to compute the internal reorganization energy using computational chemistry methods. One strategy is referred to as the '4-point' method, which was introduced by Nelsen [62]. The other is referred to as the 'direct' method. The two methods differ primarily in their ability to capture interdependence in an ET donor–acceptor pair. Application of the 4-point method implicitly assumes that the ET donor and acceptor are independent of each other, i.e., reorganization of the donor does not influence the configuration of the acceptor, and vice versa. This condition is often approximately met in an outer-sphere ET reaction wherein the donor and acceptor are not bonded to each other, or where the donor and acceptor are separated by a long molecular bridge. Mutual independence of the donor and acceptor allows one to compute λ_I from the sum of the distortion energies for the donor and acceptor separately, requiring four energy calculations (Fig. 2a) [62–66]. In contrast, in the direct method, λ_I is computed as the distortion energy for the donor-acceptor pair as an intact unit (Fig. 2b), so it captures contributions to λ_I arising from the interaction of the donor and acceptor. Hence, it is equally applicable to inner-sphere ET or ET mediated by short molecular bridge as it is to outer-sphere ET. While the direct method is more general, the 4-point method is useful because it is simpler to execute in practice.

Comparison of the performance of the 4-point and direct strategies can be of interest because it reveals the degree of interdependence between donor and acceptor, with a large difference reflecting a strongly interdependent donor–acceptor pair. For example, two comparisons have recently been given in both cases for $Fe^{II/III}$ valence interchange ET reactions in iron oxide crystals [40,51]. Electrons in some of these materials have long been viewed as spatially localized and the site-to-site motion of charge occurs by the hopping of small polarons [48]. However, the bridging of adjacent Fe atoms by one, two, and sometimes three oxygen atoms leads to the possibility of strong orbital interaction within donor-bridge-acceptor groups and the propensity for superexchange. A linear chain-like model comprised of repeating Fe^{III} O_6 octahedra (Fig. 3a) was used in one case as a representation of edge-sharing (doubly bridged) subunits of certain iron oxide crystals [51]. The chain can be described with the formula $\left[Fe^{III}(OH)_2(OH_2)_2\right]_m^{+1m}$ where m is the number of repeat units in the chain. The spin configuration on each iron atom was $t_{2g}^3 e_g^2$ and the spins were all aligned parallel (ferromagnetic). The computational tasks involved are the following: (1) determine the extent of the structural distortion associated with the creation of a single Fe^{II} ($t_{2g}^4 e_g^2$) 'defect' at some iron location in the chain, and (2) construct calculations using this distortion to compute the required energetic components of the 4-point and direct strategies as a function of ET distance along the chain. Resulting values for λ_I as a function of the ET distance are shown in Fig. 3b. For short ET distances, there are substantial differences between the results of the two strategies, indicating that the donor and acceptor are strongly interdependent. The difference decays slowly as the

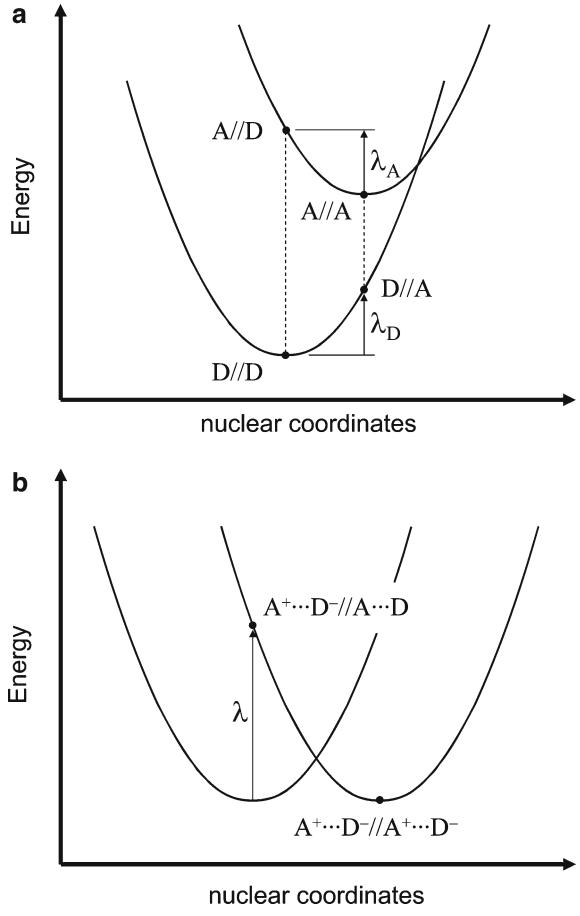

Fig. 2 Potential energy diagrams depicting the approach for using computational chemistry methods to calculate the internal reorganization energy with the **a** 4-point ($\lambda=\lambda_A+\lambda_D$) and **b** direct strategies [51,62]

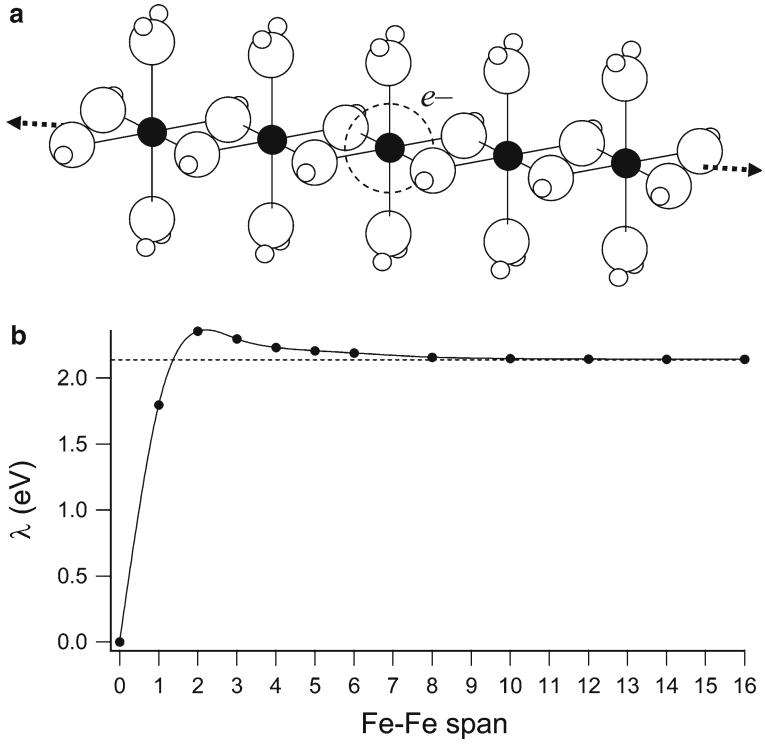

Fig. 3 Illustration of the calculated relationship between the 4-point and direct strategies for computing the internal reorganization energy [51]. A chain-like iron oxide model (**a**) was used to calculate the reorganization energy using the two different strategies (**b**) as a function of distance of separation between the ET donor and acceptor. The result for the 4-point method is shown by the *dashed line*, and the result for the direct method is shown by the *solid line*

ET distance increases, all but vanishing at distances greater than a hopping span of eight iron octahedra. At this distance, the donor and acceptor geometries are not tied to each other, and thus the 4-point method for calculating λ_I gives a good value.

3.2 External reorganization energy

The external reorganization energy pertains to the contribution of the medium, often solvent molecules, surrounding the donor–acceptor pair to the total reorganization energy. The essential task is to calculate the energy required to form the nonequilibrium (solvent) configuration appropriate for ET, while avoiding the donor and acceptor themselves. While it is possible to envision molecular simulations that include explicit solvent to assess its contribution to the reorganization energy directly [67–70], in practice a continuum model is attractive because of its simplicity. Since Marcus' famous continuum-based expression first appeared [17], many variations have been produced [71]. An example is the one allowing for ellipsoidal cavities by German and Kuznetsov [72] which, for the case of spherical cavities, gives the identical result as Marcus' expression. In this example, the external reorganization energy is given by [72]

$$\lambda_E = e^2\left(\frac{1}{\varepsilon_{opt}} - \frac{1}{\varepsilon_s}\right)\left(\frac{1}{2}\sum_{i=1}^{2}\frac{F(\varphi_i, \alpha_i)}{\sqrt{a_i^2 - c_i^2}} - \frac{1}{R}\right) \tag{11}$$

where e is the elementary charge, ε_{opt} is the optical dielectric constant, ε_s is the static dielectric constant, R is the ET distance, and $F(\phi_i\alpha_i)$ is the elliptic integral of the first kind where the parameters

$$\phi_i = \sin^{-1}\left(\frac{\sqrt{a_i^2 - c_i^2}}{a_i}\right), \tag{12}$$

and

$$\alpha_i = \sin^{-1}\sqrt{\frac{a_i^2 - b_i^2}{a_i^2 - c_i^2}}, \tag{13}$$

and a_i, b_i, c_i are the semi-axes of ellipsoid i. Despite their apparent oversimplifications, continuum-based expressions have been used with remarkable success, with their simplicity adding significantly to their value. Models with increased sophistication have been forthcoming, especially with respect to integration with current computational chemistry methods [69, 73].

3.3 Reaction coordinate: q_C

Given the equilibrium nuclear configurations for the initial and final states, an estimate of the configuration at q_C is of interest both in terms of determining the energy of the intersection and for evaluation of V_{AB}. While explicit determination of the whole reaction coordinate is desirable, it is often a

difficult task with systems possessing many nuclear degrees of freedom. Simplified, approximate reaction coordinates can be useful. One such example of utility for the two-state approach to ET is the linearized reaction coordinate model [74]. When the diabatic surfaces are parabolic, a good approximation of the reaction coordinate is given by

$$q(\xi) = \xi\, q_A + (1-\xi)\, q_B. \tag{14}$$

Using $1 \geq \xi \geq 0$, q can smoothly change from $q_A(\xi{=}1)$ to $q_B(\xi{=}0)$ going through $q_C(\xi{=}1/2)$.

3.4 Electronic coupling matrix element

The quantity V_{AB} is half of the energy splitting between the upper and lower adiabatic surfaces at q_C (Fig. 1). There are a number of strategies for estimating V_{AB} using ab initio computational methods [75]. Two strategies are briefly outlined here, namely the so-called quasi-diabatic [74] and the generalized Mulliken-Hush (GMH) [76] methods. The quasi-diabatic method is based on the conventional approach of using two diabatic states to describe the ET system. At the intersection, the splitting can be obtained by solving the secular equation

$$\begin{vmatrix} H_{AA} - E & H_{AB} - E S_{AB} \\ H_{AB} - E S_{AB} & H_{BB} - E \end{vmatrix} = 0, \tag{15}$$

where $H_{ij} = \langle \psi_i | H | \psi_j \rangle$ and i and j are equal to A or B, H is the total electronic Hamiltonian, $S_{AB} = \langle \psi_A | \psi_B \rangle$, and E is the energy eigenvalue. The two roots of the secular equation give the upper and lower adiabatic surfaces (Fig. 1). Half of the energy difference between the two adiabatic surfaces at q_C, under the simplification that $H_{AA}{=}H_{BB}$, is given by [74]

$$V_{AB} = \frac{|H_{AB} - S_{AB}\,(H_{AA} + H_{BB})\,/2|}{1 - S_{AB}^2}. \tag{16}$$

The terms may be calculated by using standard output from Hartree-Fock (HF) calculations [74]. It requires two non-orthogonal diabatic spin-unrestricted HF wavefunctions for the reactants and products. The more strongly localized these wavefunctions are, the more suitable they would be for this approach. The overlap matrix $\mathbf{D} = \mathbf{B}^{\dagger}\mathbf{S}\mathbf{A}$ is calculated from the atomic orbital overlap matrix ($\mathbf{S}$) and the eigenvectors for the two diabatic states, $\mathbf{A}$ and $\mathbf{B}$. The method of corresponding orbital transformation is used to bi–orthogonalize the overlap between the spin-orbitals of the two diabatic states, simplifying the evaluation of the Hamiltonian between them using Slater's rules [77]. The quasi-diabatic strategy has been implemented in the standard codes HONDO [78, 79] and NWChem [80].

The Mulliken-Hush method is based on the relation between the transition dipole moment μ_{12} and V_{AB} for a two-state system with weakly interacting diabatic states [20, 81]. An assumption in this method is that the diabatic states are localized, so the off-diagonal dipole moment matrix element μ_{AB} is equal to zero. This method entails, independently, defining the characteristics of the diabatic states [76]. The GMH model [76] defines the diabatic states solely in terms of adiabatic, spectroscopically observable quantities. Using the adiabatic states as a basis set for defining the diabatic states, the diabatic states are those that diagonalize the projection of the electronic dipole moment vector operator in the direction of the ET process (defined by the adiabatic dipole moment shift) [82]. The GMH expression for the electronic coupling is

$$V_{AB} = \frac{\mu_{12}\Delta E_{12}}{\left[(\Delta\mu_{12})^2 + 4(\mu_{12})^2\right]^{1/2}}, \tag{17}$$

where μ_{12} is the adiabatic transition dipole moment between states 1 and 2 and ΔE_{12} is the vertical adiabatic energy gap, and $\Delta\mu_{12}$ is the difference in the dipole moments of the adiabatic states between which the ET occurs. The GMH approach is applicable to systems with arbitrary geometries, treats excited as well as ground states, is capable of treating several states simultaneously, and permits the inclusion of electron correlation for all states of interest. All input terms are spectroscopic observables, and also can be easily extracted from electronic structure calculations.

4 Example applications

4.1 Metal ion oxidation by molecular oxygen

An example of an important environmental ET system, which has been benefited by the application of computational ET methods just discussed, is the homogeneous oxidation of aqueous transition metal ions $M^{II} \rightarrow M^{III}$ by dissolved molecular oxygen. Of particular interest is the contrast in oxidation rates of Fe^{II} and Mn^{II} hexaqua ions. The oxidation rate of these metals is generally found to be strongly pH dependent and first-order with respect to the metal ion [83]. The most widely accepted step-wise oxidation scheme that incorporates these dependencies is the Haber-Weiss mechanism [84], which can be written (ignoring waters of hydration):

$$MOH^{1+} + O_2 + H^+ \rightarrow MOH^{2+} + HO_2^{\bullet}, \tag{18}$$

$$M^{2+} + HO_2^{\bullet} + H_2O \rightarrow MOH^{2+} + H_2O_2, \tag{19}$$

$$M^{2+} + H_2O_2 \rightarrow MOH^{2+} + OH^{\bullet}, \tag{20}$$

$$M^{2+} + OH^{\bullet} \rightarrow MOH^{2+}, \tag{21}$$

where the first step involving ET from the metal ion to the molecular oxygen molecule is rate-limiting and, therefore, it is the reaction that controls the overall rate [85].

Before ET can occur, the reactants must first diffuse together to form an encounter complex. Very little is known about the structure of encounter complexes between metal ions and oxygen molecules. There is no direct evidence that would indicate whether an inner or outer-sphere complex is formed, which directly impacts the ET rate. However, analysis of the outer-sphere case is instructive and useful for comparisons with experiment. It also allows us to take advantage

Table 1 Theoretical and experimental M–O bond lengths (Å) in $M(OH_2)_6$ ions

Method	Ref.	M–O	Mn^{III}	Mn^{II} A_g	Fe^{III}	Fe^{II} A_g	Fe^{II} B_g
B3LYP/(VTZ,6-311++G**)/gas-phase	[87]	1	1.949	2.218	2.059	2.136	2.142
		2	1.949	2.218	2.059	2.137	2.143
		3	2.094	2.218	2.059	2.218	2.160
		4	2.094	2.218	2.059	2.219	2.161
		5	2.098	2.218	2.059	2.140	2.186
		6	2.098	2.218	2.059	2.143	2.186
		Avg.	2.047	2.218	2.059	2.166	2.163
B3LYP/DZVP/gas-phase	[64]		2.031	2.201	2.050	2.154	
B3LYP/6-311+G/gas-phase	[64]		2.039	2.197	2.051	2.145	
BPW86/VTZ/gas-phase	[115]		1.952(2) 2.114(4)	2.197	2.067	2.132(2) 2.127(4)	
B3LYP/(6-311+G,6-31G)/gas-phase	[89]				2.061		
Experiment	[116]			2.177	1.990	2.095	

of Marcus' cross-relation to treat the problem more easily, albeit more approximately, in terms of the self-exchange ET reactions of the separate ET couples. In one form, the cross-relation is simply [60]

$$\lambda_{12} = \frac{\lambda_{11} + \lambda_{22}}{2}, \tag{22}$$

where the subscripts are used to differentiate the reorganization energies for the cross-reaction λ_{12} and the self-exchange reactions λ_{11} and λ_{22}. For our case, then, we are interested in the self-exchange reactions

$$M(OH_2)_{6-x}(OH)_x^{3-x} + M(OH_2)_{6-x}(OH)_x^{2-x} \xrightarrow{k_{11}} M(OH_2)_{6-x}(OH)_x^{2-x} + M(OH_2)_{6-x}(OH)_x^{3-x}, \tag{23}$$

where waters of hydration are now included in the notation as are hydrolysis species, and

$$O_2 + O_2^{-\bullet} \xrightarrow{k_{22}} O_2^{-\bullet} + O_2. \tag{24}$$

The cross-reactions can be written as

$$M(OH_2)_{6-x}(OH)_x^{2-x} + O_2 \xrightarrow{k_{12}} M(OH_2)_{6-x}(OH)_x^{3-x} + O_2^{-\bullet}. \tag{25}$$

Iron ion self-exchange reactions of the type in Eq. 23 for x=0 have long been a topic of study [56,60,86]. The II/III valence interchange for $Fe(OH_2)_6$ (high-spin) involves the transfer of the minority spin electron occupying the t_{2g} subset of the Fe(3*d*) orbitals; hence, the donor orbital is of π symmetry. For the Fe^{III} hexaqua ion, five 3*d* majority spin electrons are distributed uniformly among the five 3*d* orbitals (d_{z^2}, $d_{x^2-y^2}$, d_{xy}, d_{xz}, d_{yz}). Consequently, the structure is highly symmetric (T_h symmetry). For the Fe^{II} hexaqua ion, the minority spin electron occupying the t_{2g} orbitals, which causes a Jahn-Teller distortion in the structure, breaks the symmetry. It involves the differentiation of Fe–O bond lengths into three sets of pairs, with equivalent bonds diametrically opposed from each other about the Fe atom. Slight water rotation about the Fe–O axes leads to C_{2h} symmetry [87,88]. Also, analysis of the character table for the C_{2h} point group yields two possible electron-accepting states, with symmetry labels A_g and B_g, based on whether the minority spin electron occupies the d_{xy} orbital or a mixture of d_{xz}/d_{yz}, respectively [87].

The Mn^{II} hexaqua ion shares the symmetric d^5 high-spin arrangement that is found in the Fe^{III} hexaqua ion. The $Mn^{II/III}$ valence interchange involves the transfer of one of the majority spin electrons occupying the e_g subset of the Mn(3*d*) orbitals; the donor orbital is of σ^* symmetry. Optimizations (symmetry unconstrained) of the Mn^{III} hexaqua ion yield a distorted structure involving a pair-wise differentiation of Mn–O bonds as described above, but with no water rotation, and D_{2h} symmetry [87]. Analysis of the character table for the D_{2h} point group indicates that removal of an electron from either d_{z^2} or $d_{x^2-y^2}$ orbitals of Mn^{II} yields the same irreducible representation A_g.

Standard ab initio methods such as density functional theory (DFT), particularly in the form of hybrid HF-DFT functionals such as B3LYP, can give good performance for structure prediction for these ions [64,87,89]. Accuracy in this task is one essential component for yielding good values for the (internal) reorganization energies, the other being accurate force constants. A comparison of selected calculated and experimental M–O distances is given in Table 1. For these ions, it is valid to focus primarily on the M–O distances because the single largest contribution to λ_I is from the symmetric breathing mode. Calculated bond lengths for both the Fe and Mn ions using B3LYP are slightly greater on average than from measurements of the aqueous ions using the extended X-ray absorption fine structure method (EXAFS) [90]. However, the average calculated bond length changes associated with the III→II oxidation state change are essentially identical to the 0.11 Å (Fe) [90] and 0.17 Å (Mn) [86] experimental values.

Table 2 Theoretical and experimental internal reorganization energies for $M(OH_2)_6$ ions

Method	Ref.	MnA_g	FeA_g	FeB_g
B3LYP/(VTZ,6-311++G**)/gas-phase	[87]	1.91	0.69	0.70
B3LYP/DZVP/gas-phase	[64]	2.01	0.68	
B3LYP/6-311+G/gas-phase	[64]	1.79	0.61	
B3LYP/6-311+G/PCM	[65]	2.40	0.82	
Exp.[a]		2.26	0.98	

[a] These were determined using Eq. 26 and experimental vibrational frequencies 366 cm^{-1} for Mn^{II}, 510 cm^{-1} for Mn^{III}, 388 cm^{-1} for Fe^{II}, and 506 cm^{-1} for Fe^{III} [117,118]

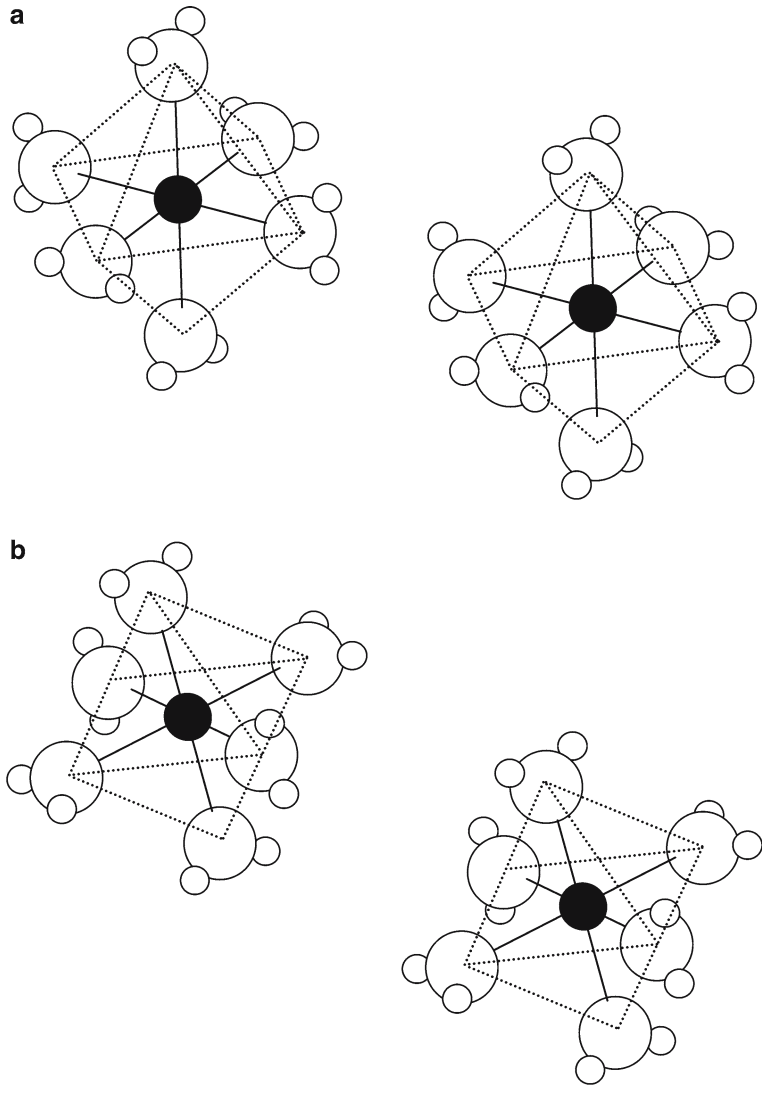

Fig. 4 Ball-and-stick diagrams of the structures and relative orientations of $M(OH_2)_6$ clusters in **a** apex-to-apex and **b** face-to-face encounter complexes [87,91]

Calculated values for λ_I demonstrate that λ_I depends primarily on the e_g versus t_{2g} nature of the donor orbital. Some recent values for λ_I computed using the 4–point method are given in Table 2. Values of λ_I analogous to experimental ones can be determined from [59]

$$\lambda_I = 3(f_{II} + f_{III})(d_{II} - d_{III})^2 \quad (26)$$

where f_i is the breathing force constant for oxidation state i, for which $f_i = 4\pi^2\nu_i^2c^2\mu$ with ν_i as the measured breathing frequency and the reduced mass μ equal to the mass of one water molecule, and d_i is a measured M–O bond distance at equilibrium. Values determined in this way are listed in Table 2 for comparison with the ab initio values.

As one source of contrast in the Fe^{II} and Mn^{II} hexaqua ion oxidation rates, the internal reorganization energy for the $Mn^{II/III}$ self-exchange ET reaction is much higher than that for the $Fe^{II/III}$ self-exchange ET reaction because the ET orbital is part of the e_g subset of the Mn($3d$) orbitals. The e_g orbitals are oriented along the Mn–O bonding directions and have strong σ–type interactions with ligand orbitals. Changing the occupation of the e_g orbitals has a large effect on the Mn–O interaction, producing large Mn–O bond-length changes and a large λ_I. The ET orbital for the $Fe^{II/III}$ self-exchange ET reaction involves the t_{2g} subset of Fe($3d$) orbitals, which are oriented along the quasi-twofold symmetry axes bisecting the octahedral edges. These orbitals do not interact strongly with ligand orbitals. Thus, changing the occupation of the Fe($3d$) t_{2g} orbitals has less influence on Fe–O bond lengths and λ_I for $Fe^{II/III}$ self-exchange ET is lower than for $Mn^{II/III}$ self-exchange ET.

The electronic coupling in $M^{II/III}(OH_2)_6$ self-exchange ET reactions is sensitive to the distance of separation and the relative orientations of the monomers in the encounter complex. Two fixed orientations that have been used for case studies are ‘apex-to-apex’ and ‘face-to-face’ orientations (Fig. 4)

Table 3 Calculated values for β and V_{AB} at selected values of r

Self-exchange ET reaction	β (Å^{-1})	$\ln V_{AB}^{r=0}$(cm^{-1})	r (Å)	V_{AB} (cm^{-1})[87]	V_{AB} (cm^{-1})[91]	V_{AB} (cm^{-1})[119]	V_{AB} (cm^{-1})[93]
Apex-to-apex							
Mn A_g	2.972	16.698	7.3	347			
Fe$A_g(d_{xy})$/B$_g(d_{xz},d_{yz})$	3.116/3.480	14.527/16.391	7.3	23/40	27	12	25
Face-to-face							
Mn A_g	2.356	9.763	5.5	27			
Fe$A_g(d_{xy})$/B$_g(d_{xz},d_{yz})$	2.534/2.242	10.171/9.715	5.5	25/35	98	50	49

[87,91]. Owing to the exponential distance dependence, the results can be compactly described by fitting to the expression [56]

$$V_{AB} = V_{AB}^{0} \exp\left[\frac{-\beta(r - r_0)}{2}\right] \quad (27)$$

where r is the separation distance, β is the decay parameter, and V_{AB}^{0} is the value of V_{AB} at the optimal separation distance r_0. Best fits to recent theoretical calculations of V_{AB} for $Fe^{II/III}$ and $Mn^{II/III}$ hexaqua ions are given in Table 3. The optimal values of r for transition metal hexaqua ion self-exchange ET are thought to be in the range of 5–9 Å [56, 60]. Newton et al. [92] have estimated r_0=5.5 Å for the Fe case. Optimal values of r for $Mn^{II/III}$ have not been determined, but values established for $Fe^{II/III}$ self-exchange can be used for $Mn^{II/III}$ to facilitate comparisons (Table 3). V_{AB} for the apex-to-apex encounter orientation is substantially larger at any given distance considered than that for the face-to-face encounter orientation, possibly due to efficient superexchange interaction mediated by the water ligands [87, 93]. Superexchange interaction may also explain, at least in part, the significant differences that exist between the Fe and Mn apex-to-apex encounter orientation relative to the face-to-face encounter orientation (Table 3).

Now we turn our attention briefly to the $O_2^{0/1-}$ self-exchange ET couple (Eq. 24). The acceptor orbital in O_2 is one of the degenerate half-filled π^* orbitals, leading to weakening of the O–O double bond upon reduction and instability in the superoxide radical product. The π^*- to π^*- match between donor–acceptor orbital symmetries make this reaction a relatively fast outer-sphere exchange [94–97]. Estimates of k_{22} based on the application of Marcus cross-relation equations to experimental cross-reaction rates have varied 16 orders of magnitude [98]. Clearly preferable is the available direct measurement [98], where use of isotopic labeling indicated that k_{22}=450±160 M^{-1} s^{-1}. Theoretical calculations have focused on various aspects of this ET reaction [65, 94, 97]. Bond-length differences between O_2 and O_2^-, as determined by DFT calculations, are predicted to be relatively large (1.254 and 1.402 Å, respectively) leading to a large λ_I given the simplicity of the structure. Using a combination of DFT structures (with PCM solvation), with r and V_{AB} calculated explicitly using semi-empirical methods [97], and using a classical expression describing the rate of encounter complex formation in aqueous solution, the self-exchange rate was estimated to be k_{22}=168 M^{-1} s^{-1} [65], in reasonably good agreement with the direct experimental measurement.

Given the above theoretical analyses of the self-exchange ET reactions, it is possible to construct a semiquantitative model for the rates of cross-reaction (Eq. 25), where the divalent metal ion is oxidized by molecular oxygen in a presumed outer-sphere encounter complex. This necessarily involves estimates of ΔG° (Fig. 1a), either by experiment or computation. Also, to assess the effects of hydrolysis on the rate, as implied in Eq. 25, the effect of changing the net molecular charge on the rate of encounter complex formation needs to be considered. Using a non-adiabatic ET treatment, calculated oxidation rates for $Fe^{II}(OH_2)_6$ are in excellent agreement with experiment (exp. $\log k_{12} = -6.0$ M^{-1} s^{-1} [30], calc. $\log k_{12} = -5.8$ M^{-1} s^{-1} [65]). In contrast, the rates calculated for the hydrolysis species of Fe^{II}, as well as those for $Mn^{II}(OH_2)_6$ and its hydrolysis species predict rates that are slower than the observed rates by two to four orders of magnitude [31,65].

The good agreement for $Fe^{II}(OH_2)_6$ is suggestive that the oxidation of this ion could follow an outer-sphere mechanism. The underprediction of the oxidation rates for the hydrolysis species of Fe^{II} and Mn^{II} indicates that a different ET mechanism is operative, likely via the creation of an inner-sphere complex. Not only are water ligand exchange rates expected to increase with increasing degrees of hydrolysis [99], but arguments based on molecular orbital theory are suggestive of an inner-sphere mechanism for Mn^{II} oxidation. The σ^* donor orbital for Mn^{II} is a poor symmetry match with the π^* acceptor orbital of O_2 for outer-sphere ET [100], but this combination is a good match for the formation of the inner-sphere adduct $[Mn(OH_2)_5(O_2)]^{2+}$ In contrast, the π symmetry of the Fe^{II} donor orbital is a match with the π^* acceptor orbital on O_2 through an outer-sphere encounter, although formation of an inner-sphere adduct is not ruled out by this analysis alone. For example, Fe^{II}–O–O bonding is found, for example, at the active site in oxyhemoglobin [101, 111,112,103], and this bonding is expected to be present in the encounter complex for the hydrolysis species of Fe^{II} [65].

4.2 Charge mobility in hematite

Injection of electrons into α–Fe_2O_3 hematite has the general outcome of converting Fe^{III} into Fe^{II}. Hence, recent theoretical ET modeling has been focused on calculating electron hopping rates specifically for this 'forced' mixed-valence condition in hematite. The essence of this ET system is a homogeneous intervalence $Fe^{II/III}$ ET (a symmetric ET,

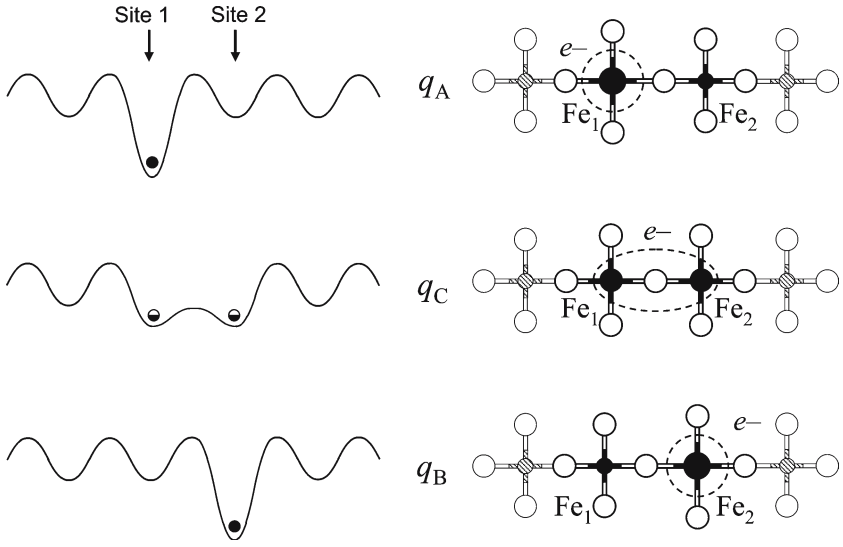

Fig. 5 Schematic illustrations of ET in solid phase iron oxides by site-to-site hopping of small polarons [40]

Fig. 1b) similar in many ways to the $Fe^{II/III}$ self-exchange ET reaction in solution as discussed earlier. An important similarity is that because electrons tend to form small polarons in hematite [48], we expect that electrons are spatially localized within the donor–acceptor pair. An important distinction from the previous system is that, in this case, the structure that becomes the donor–acceptor pair is precisely known from crystal structure information. Hematite has the corundum structure. Each Fe^{III} is coordinated to six oxygen atoms in a distorted octahedral environment. The octahedra are edge-sharing in the (001) basal plane, and face-sharing along [001]; hence, the Fe atoms in any particular nearest neighbor Fe–Fe pair are bridged by either two or three oxygen atoms. Fe–Fe distances across both the shared edges and shared faces are close to 3 Å .

The magnetic structure of hematite imposes different relevant spin configurations for ET in different crystallographic directions. Each Fe^{III} cation is in a high-spin d^5 electronic configuration. Below 960 K, the spins are ferromagnetically coupled within (001) planes and antiferromagnetically coupled along [001], yielding a net antiferromagnet nominally. In other words, in a transect along the [001] direction, every crossing of an oxygen plane is accompanied by a reversal of the majority spin direction on the iron atoms. It is interesting that although the Fe–Fe distances along [001] are nearly identical to those within (001) planes, electrical conductivity is highly anisotropic, with the least facile transport direction along [001] by up to four orders of magnitude [104]. In a classical view, the anisotropy could possibly be explained because an electron added to a lattice of high-spin (d^5) Fe^{III} atoms (a minority spin electron) is only allowed to move in an environment of parallel majority spins [48]. The minority spin electron is forbidden by Hund's rules from moving to the open shell of an adjacent spin-antiparallel Fe^{III} atom because it may not pair up in an orbital with an electron of the same spin [48, 105]. Hence, an "extra" minority-spin electron localized on any particular Fe atom would only be allowed to move to adjacent Fe atoms in the same (001) plane, and would be classically forbidden from moving along [001]. However, this "minority-spin" description is not strictly valid since electrons are fermions and electronic wavefunctions are antisymmetric with respect to the interchange of electrons. While such classical notions have been easily dispelled upon further evaluation with multi-configuration SCF methods [61], for our purposes here we will focus on the simpler case of electron transport within the parallel majority spin environment of (001) basal planes only.

A small polaron hopping model in (001) planes of hematite is easily produced using the diagram in Fig. 1b as a reference, and using HF cluster calculations in conjunction with the ET methods described above [40]. The HF approach is intrinsically inclined to produce wave functions with localized electrons because of the exclusion of the effects of electron correlation. We find this approach well suited to treatment of small polarons because of the extreme electron localization that is implied by the formation of small polarons. The initial and final diabatic states are defined as $\psi_A = Fe_1^{II}Fe_2^{III}$ and $\psi_B = Fe_1^{III}Fe_2^{II}$ (Fig. 1b). For the electron at a Fe^{II} atom to move to an adjacent Fe^{III} atom, the nuclei must first assume a configuration that achieves the electronic coincidence condition (Fig. 5). Both sites are reconfigured, and this is accomplished by thermal fluctuations in the lattice. Owing to the localized nature of the electrons in hematite, small clusters have been useful for ab initio calculation of the internal reorganization energy [40]. Tetramer clusters with composition $H_{20}Fe_4O_{16}$ (terminal protons used for charge saturation) are large enough to capture the majority of λ_I (Fig. 6). Using the direct method, the calculated λ_I=1.03 eV at the HF level. Using the continuum expression in Eqs. 11,12,13 for λ_E, a total reorganization energy of 1.20 eV was found. Using the linearized reaction coordinate model (Eq. 14) and the quasi-diabatic method (Eq. 16), calculation of the electronic coupling

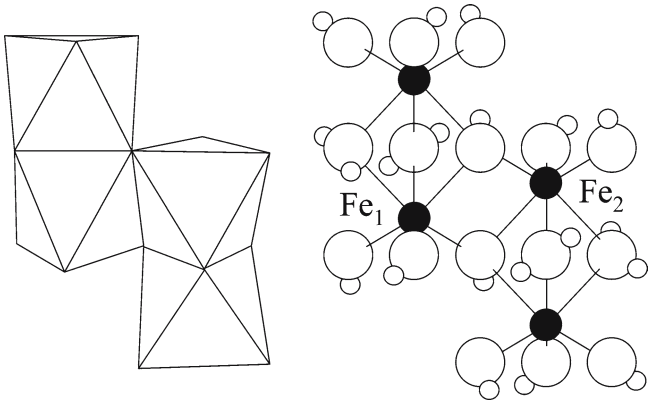

Fig. 6 Polyhedral and ball-and-stick representations of a molecular cluster used in the calculation of electron mobility in hematite [40]

matrix element at the HF level yielded 0.20 eV. Therefore, the ET turns out to be adiabatic by Eqs. 2,3,4,5, with a calculated ΔG^* of 0.11 eV [40].

To compare the calculated ΔG^* to experiment, we can use it to estimate the electron mobility within (001) planes at room temperature, an experimental observable. A slight variation of the rate expression in Eq. 10 can be used as given by [48]

$$k_{\mathrm{et}} = n\nu_n \exp\left(\frac{-\Delta G^*}{kT}\right), \tag{28}$$

where, in this case, the frequency of nuclear motion is the highest infra-red active longitudinal optic mode phonon, ν_n as 1.85E+13 s^{-1} [106], and where n is the multiplicity of nearest neighbor hopping sites for the electron. The rate k_{et} is used to estimate the diffusion coefficient D and the mobility μ using [48]

$$D = \frac{r^2 k_{\mathrm{et}}}{2}, \tag{29}$$

where r is the ET distance and

$$\mu = \frac{eD}{kT}. \tag{30}$$

The measured mobility along (001) planes in hematite is $0.10 \pm 0.02\ \mathrm{cm}^2\,\mathrm{V}^{-1}\,\mathrm{s}^{-1}$ [107]. The calculated mobility is $0.06\ \mathrm{cm}^2\,\mathrm{V}^{-1}\,\mathrm{s}^{-1}$ [40]. Various other experimental methods give indirect estimates of the activation energy, placing it close to 0.1 eV [48,108,109]. The good agreement attests to the success of the small polaron ET model for capturing the essential physics of the hematite ET system.

5 Future directions

Despite advances that have been made on the two highlighted environmental ET systems, much work remains to be done. Direct computation of the free energy surfaces for the metal ion oxidation reactions, perhaps by molecular dynamics simulations and umbrella sampling [67,68], would yield the ET driving force as well as the activation energy simultaneously. Such methods could also be useful for determining optimal distances of separation for ET in this system as well. Perhaps more importantly, however, is describing the oxidation rate of inner-sphere ET, which would ideally include simulation of the rate of formation of inner-sphere encounter complexes. In case of slow ligand exchange rates, we might consider use of transition path sampling methods for the simulation of such rare events [110]. For ET in hematite, the calculations need to be adapted to iron environments near the solid surface equilibrated with aqueous solution, where electrostatic fields associated with the solid–water interface presumably would bias the random walk of injected electrons. In this regard, we envision the utility of kinetic Monte Carlo simulations of the dynamics of electron hopping, with the effects of electrostatic fields incorporated and with parameters based on ab initio calculations of elementary ET hopping processes.

In a broader perspective, the situation is much more inexhaustible. Our understanding of the kinetics in many environmental ET systems is disadvantaged by a lack of theoretical analysis. The advances in simulation of elementary ET processes that are being made in other disciplines such as molecular biology [60,111–113] are relevant to, and will benefit, research on environmental ET systems. For instance, recent efforts to model ET in metalloproteins using large-scale high-level calculations such as combined quantum and molecular mechanics (QM/MM) methods are forging the way for similar efforts on ET proteins in the electron transport chain in metal-reducing bacteria [114]. These kinds of modeling efforts exemplify the ultimate goal of many-atom simulations of environmental ET processes at the quantum mechanical level. We think such goals are obtainable now both in terms of existing theories and computational hardware. The main limitation seems to be manpower. Hence we are enthusiastically engaged in helping to push forward the environmental sciences one step at a time.

Acknowledgements This work was made possible by a grant from the U.S. Department of Energy, Office of Basic Energy Sciences, Engineering and Geosciences Division. This research was performed in part using the Molecular Science Computing Facility (MSCF) in the William R. Wiley Environmental Molecular Sciences Laboratory at the Pacific Northwest National Laboratory. The MSCF is funded by the Office of Biological and Environmental Research in the U.S. Department of Energy. Pacific Northwest National Laboratory is operated by Battelle for the U.S. Department of Energy under Contract DE-AC06-76RLO 1830.

References

1. Stumm W, Morgan JJ (1981) Aquatic chemistry. Wiley, New York
2. Zachara JM, Fredrickson JK, Li SM, Kennedy DW, Smith SC, Gassman PL (1998) Am Mineral 83:1426
3. Rosso KM, Smith DMA, Wang ZM, Ainsworth CC, Fredrickson JK (2004) J Phys Chem 108:3292
4. Newman DK, Kolter R (2000) Nature 405:94
5. Nurmi JT, Tratnyek PG (2002) Environ Sci Technol 36:617
6. Maurice PA, Hochella MF Jr, Parks GA, Sposito G, Schwertmann U (1995) Clays Clay Miner 43:29

7. Stone AT, Morgan JJ (1987) In: Stumm W (ed) Aquatic surface chemistry, Wiley, New York, p 221
8. Ilton ES, Haiduc A, Moses CO, Heald SM, Elbert DC, Veblen DR (2004) Geochim Cosmochim Acta 68:2417
9. Peterson ML, White AF, Brown GE Jr, Parks GA (1997) Environ Sci Technol 31:1573
10. Cui DQ, Eriksen TE (1996) Environ Sci Technol 30:2263
11. Scott MJ, Morgan JJ (1996) Environ Sci Technol 30:1990
12. Elsner M, Haderlein SB, Kellerhals T, Luzi S, Zwank L, Angst W, Schwarzenbach RP (2004) Environ Sci Technol 38:2058
13. Strathmann TJ, Stone AT (2003) Geochim Cosmochim Acta 67:2775
14. Pecher K, Haderlein SB, Schwarzenbach RP (2002) Environ Sci Technol 36:1734
15. Amonette JE, Workman DJ, Kennedy DW, Fruchter JS, Gorby YA (2000) Environ Sci Technol 34:4606
16. Butler EC, Hayes KF (1998) Environ Sci Technol 32:1276
17. Marcus RA (1956) J Chem Phys 24:966
18. Sutin N (1962) Annu Rev Nucl Sci 12:285
19. Dogonadze RR, Kuznetsov AM, Zakaraya MG, Ulstrup J, Inst Electrochem MU (1979) Tunneling Biol Syst [Proc Symp], p 145
20. Hush NS (1967) Prog Inorg Chem 8:391
21. Bricker O (1965) Am Mineral 50:1296
22. Diem D, Stumm W (1984) Geochim Cosmochim Acta 48:1571
23. Singer PC, Stumm W (1970) Science 167:1121
24. Lowson RT (1982) Chem Rev 82:461
25. Millero FJ (1985) Geochim Cosmochim Acta 49:547
26. Millero FJ, Sotolongo S, Izaguirre M (1987) Geochim Cosmochim Acta 51:793
27. Millero FJ, Izaguirre M (1989) J Sol Chem 18:585
28. Millero FJ (1989) Mar Chem 28:1
29. King DW, Lounsbury HA, Millero FJ (1995) Environ Sci Technol 29:818
30. King DW (1998) Environ Sci Technol 32:2997
31. Morgan JJ (2005) Geochim Cosmochim Acta 69:35
32. Hem JD (1963) US Geol Soc Water Supp 1667-A:A1
33. Morgan JJ (1967) In: Faust S, Hunter J (eds) Principles and applications of water chemistry. Wiley, New York, p 561
34. Sellers RM, Simic MG (1976) J Am Chem Soc 98:6145
35. Bakac A, Espenson JH (1993) Acc Chem Res 26:519
36. Bakac A, Scott SL, Espenson JH, Rodgers KR (1995) J Am Chem Soc 117:6483
37. Mulvaney P, Swayambunathan V, Grieser F, Meisel D (1988) J Phys Chem 92:6732
38. Mulvaney P, Cooper R, Grieser F, Meisel D (1988) Langmuir 4:1206
39. Mulvaney P, Swayambunathan V, Grieser F, Meisel D (1990) Langmuir 6:555
40. Rosso KM, Smith DMA, Dupuis M (2003) J Chem Phys 118:6455
41. Williams AGB, Scherer MM (2004) Environ Sci Technol 38:4782
42. Rosso KM, Zachara JM, Fredrickson JK, Gorby YA, Smith SC (2003) Geochim Cosmochim Acta 67:1081
43. Freier S, Greenshpan P, Hillman P, Shechter H (1962) Phys Lett 2:191
44. Lielmezs J, Chaklader ACD (1965) J Appl Phys 36:866
45. Ma Y, Johnson PD, Wassdahl N, Guo J, Skytt P, Nordgren J, Kevan SD, Rubensson J-E, Boske T, Eberhardt W (1993) Phys Rev B 48:2109
46. Mochizuki S (1977) Physica Status Solidi A 41:591
47. Morin FJ (1954) Phys Rev 93:1195
48. Goodenough JB (1971) In: Reiss H (ed) Progress in solid state chemistry, vol 5. Pergamon Press, Oxford, p 149
49. Dimitrijevic NM, Savic D, Micic OI, Nozik AJ (1984) J Phys Chem 88:4278
50. Cherepy NJ, Liston DB, Lovejoy JA, Deng HM, Zhang JZ (1998) J Phys Chem B 102:770
51. Rosso KM, Dupuis M (2004) J Chem Phys 120:7050
52. Sherman DM (1987) Phys Chem Miner 14:355
53. Franck J (1925) Trans Faraday Soc 21:536
54. Condon EU (1928) Phys Rev 32:858
55. Sutin N (1986) In: Zuckermann JJ (ed) Electron transfer and electochemical reactions; photochemical and other energized reactions, vol 15. VCH, New York, p 16
56. Newton MD, Sutin N (1984) Ann Rev Phys Chem 35:437
57. Landau L (1932) Phys Z Sowjet 1:89
58. Zener C (1932) Proc Roy Soc A137:696
59. Brunschwig BS, Logan J, Newton MD, Sutin N (1980) J Am Chem Soc 102:5798
60. Marcus RA, Sutin N (1985) Biochim Biophys Acta 811:265
61. Iordanova N, Dupuis M, Rosso KM (2005) J Chem Phys 122:144305
62. Nelsen SF, Blackstock SC, Kim Y (1987) J Am Chem Soc 109:677
63. Klimkans A, Larsson S (1994) Chem Phys 189:25
64. Rosso KM, Rustad JR (2000) J Phys Chem A 104:6718
65. Rosso KM, Morgan JJ (2002) Geochim Cosmochim Acta 66:4223
66. Zhang XD, Wang YN, Guo JX, Zhang QY (1999) J Photochem Photobiol A Chem 121:1
67. Kuharski RA, Bader JS, Chandler D, Sprik M, Klein ML, Impey RW (1988) J Chem Phys 89:3248
68. Rustad JR, Rosso KM, Felmy AR (2004) J Chem Phys 120:7607
69. Ando K (2001) J Chem Phys 115:5228
70. Vener MV, Leontyev IV, Basilevsky MV (2003) J Chem Phys 119:8038
71. Brunschwig BS, Ehrenson S, Sutin N (1986) J Phys Chem 90:3657
72. German ED, Kuznetsov AM (1981) Electrochim Acta 26:1595
73. Leontyev IV (2004) Theor Chem Acc 111:110
74. Farazdel A, Dupuis M, Clementi E, Aviram A (1990) J Am Chem Soc 112:4206
75. Amini A, Harriman A (2003) J Photochem Photobiol C 4:155
76. Cave RJ, Newton MD (1996) Chem Phys Lett 249:15
77. King HF, Stanton RE, Kim H, Wyatt RE, Parr RG (1967) J Chem Phys 47:1936
78. Dupuis M, Rys J, King HF (1976) J Chem Phys 65:111
79. Dupuis M (2001) Comp Phys Comm 134:150
80. Apra E, Bylaska EJ, de Jong W, Hackler MT, Hirata S, Pollack L, Smith DMA, Straatsma TP, Windus TL, Harrison RJ, Nieplocha J, Tipparaju V, Kumar M, Brown E, Cisneros G, Dupuis M, Fann GI, Fruchtl H, Garza J, Hirao K, Kendall R, Nichols JA, Tsemekhman K, Valiev M, Wolinski K, Anchell J, Bernholdt D, Borowski P, Clark T, Clerc D, Dachsel H, Deegan M, Dyall K, Elwood D, Glendening E, Gutowski M, Hess A, Jaffe J, Johnson B, Ju J, Kobayashi H, Kutteh R, Lin Z, Littlefield R, Long X, Meng B, Nakajima T, Niu S, Rosing M, Sandrone G, Stave M, Taylor H, Thomas G, van Lenthe J, Wong A, Zhang Z (2003) NWChem: a computational chemistry package designed to run on high-performance parallel supercomputers, version 4.5 (Pacific Northwest National Laboratory)
81. Mulliken RS (1952) J Am Chem Soc 64:811
82. Newton MD (2003) Coord Chem Rev 238:167
83. Stumm W, Morgan JJ (1996) Aquatic chemistry. Wiley, New York
84. Haber F, Weiss J (1934) Proc Roy Soc London A147:332
85. Fallab S (1967) Angew Chem Int Ed 6:496
86. Creutz C, Sutin N (1986) In: Zuckermann JJ (ed) Electron-transfer and electochemical reactions; photochemical and other energized reactions, vol 15. VCH, New York, p 47
87. Rosso KM, Smith DMA, Dupuis M (2004) 108:5242
88. Rosso KM, Rustad JR, Gibbs GV (2002) J Phys Chem A 106:8133
89. Martin RL, Hay PJ, Pratt LR (1998) J Phys Chem A 102:3565
90. Sham TK, Hastings JB, Perlman ML (1981) Chem Phys Lett 83:391
91. Logan J, Newton MD (1983) J Chem Phys 78:4086
92. Tembe BL, Friedman HL, Newton MD (1982) J Chem Phys 76:1490
93. Newton MD (1988) J Phys Chem 92:3049
94. Ohta K, Morokuma K (1987) J Phys Chem 91:401
95. Bu YX, Liu CB (1999) J Mol Struct Theochem 490:7
96. Bu YX, Sun HT, Niu HB (1999) J Comp Chem 20:989
97. German ED, Kuznetsov AM, Efremenko I, Sheintuch M (1999) J Phys Chem A 103:10699

98. Lind J, Shen X, Merenyi G, Jonsson BO (1989) J Am Chem Soc 111:7654
99. Richens DT (1997) The chemistry of aqua ions, Wiley, New York
100. Luther GW III (1990) In: Stumm W (ed) Aquatic chemical kinetics. Wiley, New York City, p 173
101. Goddard WA, Olafson BD (1975) Proc Natl Acad Sci USA 72:2335
102. Olafson BD, Goddard WA (1977) Proc Natl Acad Sci USA 74:1315
103. Scherlis DA, Estrin DA (2002) Int J Quantum Chem 87:158
104. Nakau T (1960) J Phys Soc Jpn 15:727
105. Cox PA (1980) Chem Phys Lett 69:340
106. Tsuda N, Nasu K, Fujimori A, Siratori K (2000) Electronic conduction in oxides, vol 94. Springer, Berlin Heidelberg New York
107. van Daal HJ, Bosman AJ (1967) Phys Rev 158:736
108. Papaioannou JC, Patermarakis GS, Karayianni HS (2005) J Phys Chem Solids 66:839
109. Gleitzer C (ed) (1997) Electrical properties of oxide materials, vol 125–126. Trans Tech Publications, Switzerland, p 355
110. Bolhuis PG, Chandler D, Dellago C, Geissler PL (2002) Annu Rev Phys Chem 53:291
111. Fedurco M (2000) Coord Chem Rev 209:263
112. Gray HB, Winkler JR (2003) In: Kadish KM, Smith KM, Guilard R (eds) The Porphyrin Handbook, vol 11. Elsevier, p 51
113. Kuznetsov AM, Ulstrup J (2004) J Electroanal Chem 564:209
114. Smith DMA, Dupuis M, Vorpagel ER, Straatsma TP (2003) J Am Chem Soc 125:2711
115. Li J, Fisher CL, Chen JL, Bashford D, Noodleman L (1996) Inorg Chem 35:4694
116. Sham TK, Hastings JB, Perlman ML (1980) J Am Chem Soc 102:5904
117. Kanno H (1988) J Phys Chem 92:4232
118. Johnson DA, Nelson PG (1999) Inorg Chem 38:4949
119. Newton MD (1986) J Phys Chem 90:3734